Original Article

Institution of MECHANICAL ENGINEERS

Journal of AUTOMOBILE ENGINEERING

Proc IMechE Part D:
J Automobile Engineering
1–19

DOI: 10.1177/0954407015586076
pid.sagepub.com
SAGE

An inertial delay observer-based sliding mode control for active suspension systems

Sunny Gupta, Divyesh Ginoya, P D Shendge and Shrivijay B Phadke

Abstract

In this paper, an active suspension system based on an inertial delay observer combined with sliding mode control is proposed for a quarter-car model. The inertial delay observer estimates the states and the uncertainties and disturbances of a system simultaneously. It is an extension of the inertial delay control which estimates the uncertainties of a system but needs the measurement of all states. The proposed scheme needs only the sprung mass position sensor for its implementation. The overall stability of the system is proved. The scheme is validated by simulation and by experimentation on a laboratory set-up. The results obtained with the proposed scheme are compared with those obtained with a passive suspension scheme, an linear quadratic Gaussian observer-based scheme and an inertial delay control-based scheme.

Keywords

active suspension, inertial delay control, inertial delay observer, sliding mode control

Date received: 23 July 2014; accepted: 8 April 2015

Introduction

The main function of a suspension system is to isolate the passengers from the road disturbance. The performance of a passive suspension system under varying road profiles is limited due to the fixed nature of its configuration. In contrast, an active suspension system which introduces a force generator in parallel with the passive suspension components such as springs and dampers, has a greater flexibility to deal with different road profile scenarios. However, The design of an active suspension system is beset with several problems. The knowledge of system components such as the springs and the dampers is often inaccurate, the sprung mass may not be constant and the road profile may have a wide variation. Further all signals required for generating the control law may not be available.

In the past, many control strategies have been proposed in the literature to overcome some of the challenges in the design of an active suspension system. The application of optimal control,[1] linear quadratic regulator-based control,[2] adaptive and model reference adaptive control,[3–9] are some of the strategies that are reported in the literature. Recently some strategies that focus on integrated control of steering and active suspension,[10] active suspension and braking[11] are reported. Since it is difficult to get an accurate model of a suspension system, many researchers have employed control strategies that do not require any model or require only a crude model of a system. Fuzzy control which does not need a model is applied to active suspension in Rajeswari and Lakshmi,[12] its combination with neural networks has been described by Al-Holou et al.[13] and Esat et al.[14] Sliding mode control (SMC) can work with a model in which only the range of uncertainties and the bounds of disturbances is known. SMC and its combinations applied to active suspension have been reported by Mohan et al.,[8,9] Kim and Ro,[15] Lin et al.[16] and Lian.[17] Some strategies based on the estimation of uncertainties such as the inertial delay control (IDC)[18] and the disturbance observer[19] applied to the active suspension are also reported.

As far as the sensor measurements are concerned the strategies mentioned above require sensors for measurement of displacements and velocities of the sprung and unsprung masses. It is particularly difficult to get the transducers capable of measurement of skyhook

College of Engineering Pune, Pune, India

Corresponding author:
Shrivijay B Phadke, College of Engineering Pune, 5 Wellesley Road, Shivajinagar, Pune 411005, India.
Email: sbp.instru@coep.ac.in

velocity or velocity signal in general.[20] The velocity signal can be obtained by passing the displacement signal through a high-pass filter or by numerical differentiation. The solutions reported in the literature based on integration of the vertical acceleration and similar approaches can be seen in Truscott,[6] Lin et al.[16] and Preumont et al.[21] A capacitive microelectromechanical system (MEMS) velocity sensor to get the skyhook velocity is given in Alshehri et al.[22]

A general solution to obtain the states is to use an observer. A simple Luenberger observer is unlikely to work satisfactorily for an active suspension system because of uncertainties and wide ranging road disturbances which are unknown. Use of special sensors to get this information directly or by using lead vehicles as sensors can be seen in the literature. A vehicle-mounted preview sensor is employed by Abdel-Hady[23] and Ryu et al.,[24] whereas using a lead vehicle in a convoy as a preview sensor is proposed by Rahman and Rideout.[25] A nonlinear observer,[26] adaptive observer,[5] a sliding mode observer[27] for semi-active suspension, an observer-based fuzzy sliding observer,[28,29] LQG-based[30] are some of the examples of the use of observer for active suspension. An estimator based suspension system for controlling the motorized suspension damper is proposed in Seo et al.[31]

The focus of this paper is on designing an active suspension system that estimates the states of the system in addition to estimating the effect of uncertainties and road disturbance. The main motivation for the simultaneous estimation of states and uncertainty is to reduce the number of sensors and to robustify the control in the presence of unknown road disturbance and uncertainties in the system parameters. The time delay control, the IDC, also known as uncertainty and disturbance estimator,[32–35] are methods to estimate the uncertainties and disturbances using past measurements. These methods need the states of the system. An inertial delay observer (IDO) to estimate the uncertainties and states of the system is reported without a stability proof in Ginoya et al.[36]

The work reported by Deshpande et al.[18] estimates the effect of uncertainties and road disturbance but needs the positions and velocities of sprung mass as well as unsprung mass. Deshpande et al.[19] the effect of uncertainties and road disturbance is estimated using the position and velocity of just the sprung mass, thereby reducing the sensor requirement by two. This paper takes the work of Deshpande et al.[18,19] forward by estimating the effect of uncertainties and road disturbance and the states of the sprung mass using just the position of sprung mass. Usually getting a good measurement of the velocities of the sprung mass or unsprung mass is difficult and the road profiles can change significantly even for short runs. The proposed scheme can estimate the velocity of the sprung mass obviating the need for its measurement and the estimation of the effect of road disturbances and uncertainties obviates the need for special preview sensors.

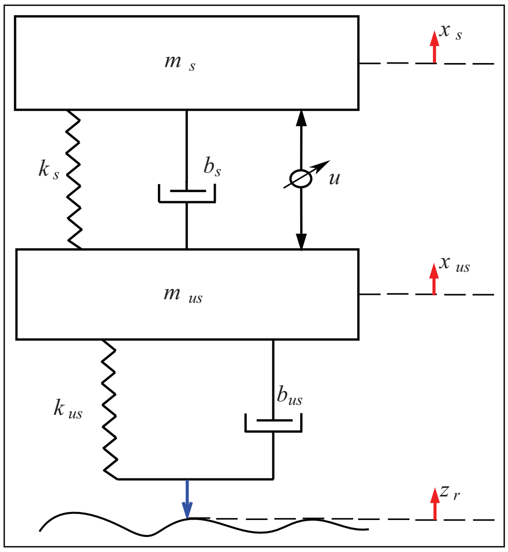

Figure 1. Quarter-car suspension model.

The main features of the proposed paper are:

1. a single-sensor-based active suspension system;
2. simultaneous estimation of states of the sprung mass and the effect of uncertainties and road disturbance;
3. stability of overall system is proved;
4. experimental validation of the proposed control.

The rest of the paper is organized as follows: Section 2 describes the problem, Section 3 gives a brief introduction to IDC, Section 4 develops the IDO and the SMC, Section 5 derives the stability of the overall system, Section 6 gives the simulation results while Section 7 validates the proposed control on hardware and Section 8 summarizes the conclusions.

Problem statement

In this section, the dynamic model of the active suspension system is derived. A quarter-car model is considered to describe the system dynamics. The schematic diagram of a quarter-car suspension system is shown in Figure 1. The sprung mass m_s represents the mass of the vehicle body and passengers, the unsprung mass m_{us} represents the mass of the tire, wheel, break and the suspension linkage. The spring k_s and the damper b_s are the components of the passive suspension system which support the body weight over the tire. The spring k_{us} and the damper b_{us} model the stiffness of the tire which is in contact with the road. An actuator is placed between the sprung mass and the unsprung mass. The actuator generates the control force to minimize the acceleration and displacement of the sprung mass which improves the ride comfort. The road disturbance is denoted by z_r.

The equations of motion for the sprung mass and the unsprung mass can be written as

$$m_s\ddot{x}_s = -k_s(x_s - x_{us}) - b_s(\dot{x}_s - \dot{x}_{us}) + u \tag{1}$$

$$\begin{aligned} m_{us}\ddot{x}_{us} &= k_s(x_s - x_{us}) + b_s(\dot{x}_s - \dot{x}_{us}) \\ &\quad - k_{us}(x_{us} - z_r) - b_{us}(\dot{x}_{us} - \dot{z}_r) - u \end{aligned} \tag{2}$$

where u is the control force generated by the actuator. Denoting the states of the system as $x_1 = x_s$, $x_2 = \dot{x}_s$, $x_3 = x_{us}$, $x_4 = \dot{x}_{us}$ and writing the system dynamics in the state space form as

$$\left.\begin{aligned} \dot{x}_1 &= x_2 \\ \dot{x}_2 &= -\frac{k_s}{m_s}x_1 - \frac{b_s}{m_s}x_2 + \frac{k_s}{m_s}x_3 + \frac{b_s}{m_s}x_4 + \frac{1}{m_s}u \\ \dot{x}_3 &= x_4 \\ \dot{x}_4 &= \frac{k_s}{m_{us}}x_1 + \frac{b_s}{m_{us}}x_2 - \frac{(k_s + k_{us})}{m_{us}}x_3 - \frac{(b_s + b_{us})}{m_{us}}x_4 + \frac{k_{us}}{m_{us}}z_r + \frac{b_{us}}{m_{us}}\dot{z}_r - \frac{1}{m_{us}}u \end{aligned}\right\} \tag{3}$$

The objective of the design of control is to improve the ride comfort by trying to make the sprung mass acceleration small in spite of uncertainties in the suspension system and in the presence of road disturbance. Further this is to be accomplished using only the sprung mass displacement information.

Inertial delay control

In this section, the concept of IDC is explained in brief. The controller is designed here along the lines of Deshpande et al.[18] and Talole and Phadke,[34] where the IDC is combined with SMC. The basic idea of IDC is to estimate the effect of uncertainties and disturbances by using the system information in the recent past. The reason for explaining the IDC is to provide the background for the development of an IDO given in Section 4.

The sliding surface is formulated using the sprung mass displacement x_1 and velocity x_2 as

$$\sigma = cx_1 + x_2 \tag{4}$$

where $c > 0$ is a user chosen constant. Differentiating (4) and using (3),

$$\dot{\sigma} = cx_2 - \frac{k_s x_1}{m_s} - \frac{b_s x_2}{m_s} + \frac{k_s x_3}{m_s} + \frac{b_s x_4}{m_s} + \frac{u}{m_s} \tag{5}$$

Defining

$$e = -k_s x_1 - b_s x_2 + k_s x_3 + b_s x_4 \tag{6}$$

and using it in (5) gives

$$\dot{\sigma} = c\,x_2 + h\,e + h\,u \tag{7}$$

where $h = \frac{1}{m_s}$. Note that the expression for e may contain the uncertainties in the spring and the damper coefficients and the effect of the road disturbance coming through the unsprung mass position x_3 and velocity x_4. The variable e is called the lumped uncertainty. The idea here is to estimate e using the IDC and to use the opposite of the estimate in u.

Selecting the control input to stabilize the system as

$$u = u_{eq} + u_n \tag{8}$$

where u_{eq} is designed to cater for the known terms present in (7) and is given by

$$u_{eq} = -\frac{1}{b}\left[c\,x_2 + k\,\sigma\right] \tag{9}$$

where $k > 0$ is a user chosen constant. Using (8) and (9) in (7)

$$\dot{\sigma} = bu_n + be - k\sigma \tag{10}$$

Let $\hat{e}$ be the estimate of the lumped uncertainty e, which is estimated by passing e through a broad-band filter $G_f(s)$ given by

$$G_f(s) = \frac{1}{\tau s + 1} \tag{11}$$

where $\tau > 0$ is the filter time constant. Now selecting u_n as

$$u_n = -\hat{e} \tag{12}$$

Using (10), (11) and (12) the estimate of the lumped uncertainty works out to

$$\hat{e} = \frac{1}{b\,\tau}\left(\sigma + k\int_0^t \sigma\,dt\right) \tag{13}$$

A block schematic of the IDC based SMC is shown in Figure 2. Defining the estimation error as $\tilde{e} = e - \hat{e}$, the dynamics of sliding variable σ becomes

$$\dot{\sigma} = b\tilde{e} - k\sigma \tag{14}$$

It has been shown by Deshpande et al.[18] that the sliding variable σ is ultimately bounded whereby ride comfort can be assured. However the control requires the sprung mass position x_1 as well as sprung mass velocity x_2. In the next section an IDO is designed to overcome the need to measure the sprung mass velocity x_2.

Inertial delay observer and controller

In this section, an IDO is designed to estimate the sprung mass position x_1, sprung mass velocity x_2 and the lumped uncertainty simultaneously and then the estimated states and the estimate of uncertainty is used to implement the controller and in the next section the stability of the overall system is proved. The sprung mass displacement x_1 is assumed to be the only signal available for measurement.

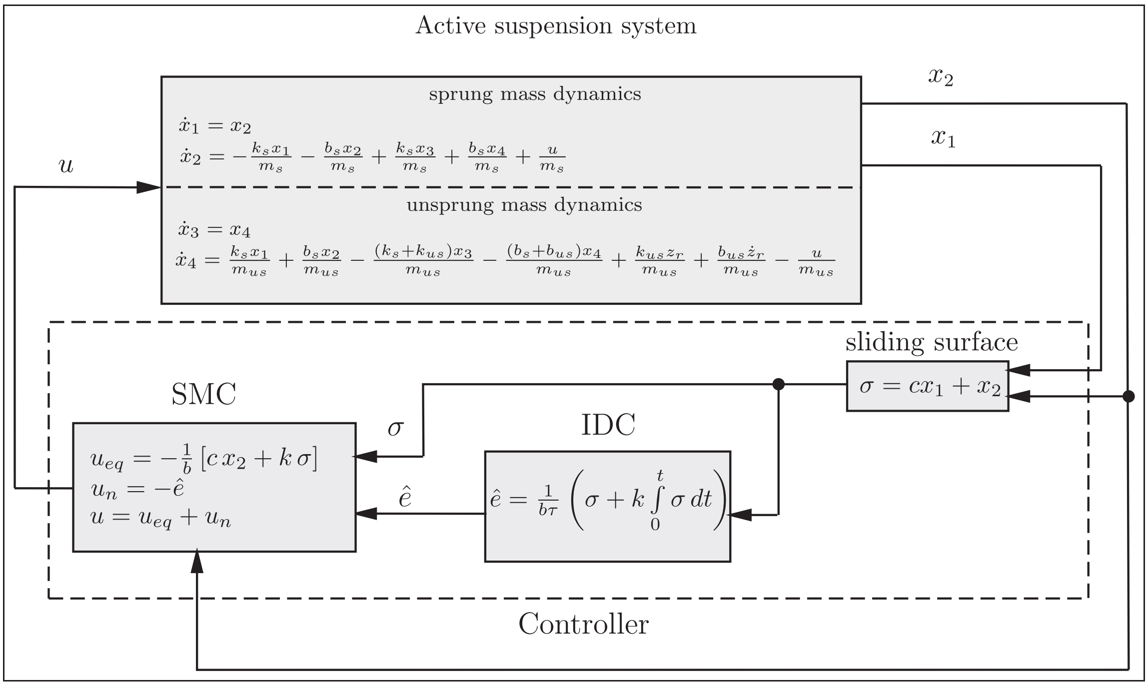

Figure 2. IDC-based SMC scheme.

IDO

Consider the dynamics of sprung mass given in (3),

$$\left.\begin{aligned}\dot{x}_1 &= x_2\\ \dot{x}_2 &= -\frac{k_s x_1}{m_s} - \frac{b_s x_2}{m_s} + \frac{k_s x_3}{m_s} + \frac{b_s x_4}{m_s} + \frac{u}{m_s}\end{aligned}\right\} \tag{15}$$

Writing the dynamics of sprung mass in compact form as

$$\left.\begin{aligned}\dot{x} &= Ax + Bu + Be\\ y &= Cx\end{aligned}\right\} \tag{16}$$

where the system parameter matrices are given by

$$A = \begin{bmatrix} 0 & 1 \\ 0 & 0 \end{bmatrix}; \quad B = \begin{bmatrix} 0 \\ \frac{1}{m_s} \end{bmatrix}; \quad C = [1 \quad 0]$$

The state vector is given by $x = [x_1 \quad x_2]^T$ and the lumped uncertainty e is as given in (6). The dynamics of the observer is chosen as

$$\left.\begin{aligned}\dot{\hat{x}} &= A\hat{x} + Bu + B\hat{e} + L(y - \hat{y})\\ \hat{y} &= C\hat{x}\end{aligned}\right\} \tag{17}$$

where $\hat{x}$ is the estimate of the state vector x, $\hat{e}$ is the estimate of the lumped uncertainty e and L is the observer gain. Notice the addition of $B\hat{e}$ in (17) enabling improvement over the classical Luenburger observer. One can write the estimate of lumped uncertainty using (16) as

$$e = B^+[\dot{x} - Ax - Bu] \tag{18}$$

where $B^+ = (B^T B)^{-1} B^T$ is the pseudo-inverse of matrix B. If the states x_1, x_2 were available for measurement, the lumped uncertainty could have been estimated using (18) as explained in Section 3. However since the states are not available for measurement, x is replaced by $\hat{x}$ in (18) giving

$$\bar{e} = B^+[\dot{\hat{x}} - A\hat{x} - Bu] \tag{19}$$

The estimate of the lumped uncertainty $\hat{e}$ is expressed as

$$\hat{e} = G_f(s)\,\bar{e} \tag{20}$$

where $G_f(s)$ is a broad-band filter. Using (17), (19) and (20), the update law for the estimate $\hat{e}$ can be obtained as

$$\dot{\hat{e}} = \frac{1}{\tau} B^+ L(y - \hat{y}) \tag{21}$$

Defining the state estimation error as $\tilde{x} = x - \hat{x}$ and the disturbance estimation error as $\tilde{e} = e - \hat{e}$ and writing the dynamics of state estimation error using (16) and (17) as

$$\dot{\tilde{x}} = (A - LC)\tilde{x} + B\tilde{e} \tag{22}$$

Subtracting $\dot{e}$ from both sides of (21) gives

$$\dot{\tilde{e}} = -\frac{1}{\tau} B^+ LC\tilde{x} + \dot{e} \tag{23}$$

Assumption 1. *The lumped uncertainty e is continuous and satisfies*

$$\left|\frac{de}{dt}\right| < \mu \tag{24}$$

where μ is a positive unknown number.

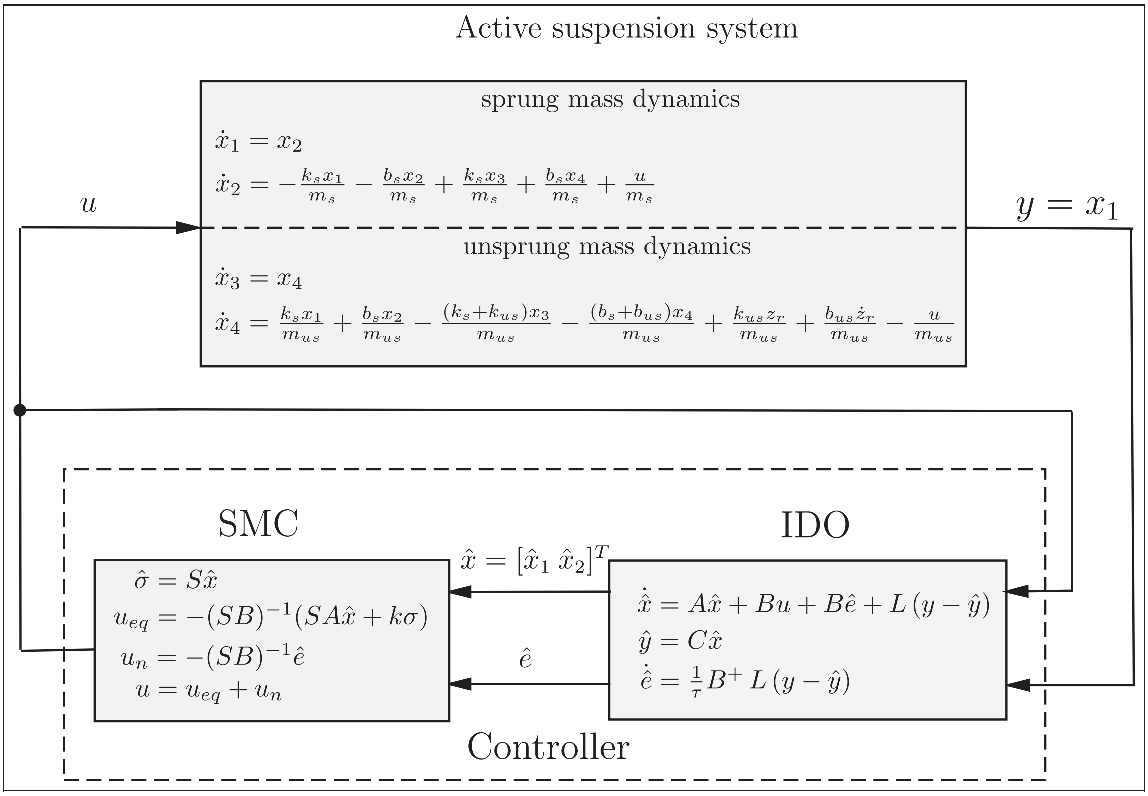

Figure 3. IDO-based SMC scheme.

This assumption admits a fairly large class of uncertainties and road disturbances. It may be noted that the design of control does not need the actual value of μ. Writing the observer error dynamics in compact form using (22), (23),

$$\dot{\tilde{z}} = M\tilde{z} + N\dot{e} \tag{25}$$

where

$$\tilde{z} = \begin{bmatrix} \tilde{x} \\ \tilde{e} \end{bmatrix}; \quad M = \begin{bmatrix} A - LC & B \\ -\frac{1}{\tau}B^+ LC & 0 \end{bmatrix}; \quad N = \begin{bmatrix} 0 \\ 0 \\ 1 \end{bmatrix}$$

The stability analysis of the observer is discussed in Section 5. Next the SMC is design based on the observer states and the estimate of the lumped uncertainty.

Controller design

The sliding surface is defined now using the observer states as

$$\hat{\sigma} = S\hat{x} \tag{26}$$

where the vector is defined as $S = [c\ 1]$. Differentiating (26) and using (16)

$$\dot{\hat{\sigma}} = S[A\hat{x} + Bu + B\hat{e} + L(y - \hat{y})] \tag{27}$$

The control input u is split into two parts as

$$u = u_{\text{eq}} + u_n \tag{28}$$

with

$$u_{\text{eq}} = -(SB)^{-1}(SA\hat{x} + k\hat{\sigma}) \tag{29}$$

$$u_n = -(SB)^{-1}\hat{e} \tag{30}$$

where the estimate of lumped disturbance is given in (21). A block schematic of the IDO-based SMC is shown in Figure 3. The dynamics of $\hat{\sigma}$ becomes

$$\dot{\hat{\sigma}} = SLC\tilde{x} - k\hat{\sigma} \tag{31}$$

The stability analysis of the observer and the closed-loop system is given in the next section.

Stability

In this section, the stability analysis of the observer and the overall system are given in the sense of ultimate boundedness presented in Corless and Leitmann.[37] The stability proof derived here aiming for ultimate boundedness of all signals. From (25), it can be seen that one can place the eigenvalues of M arbitrarily by selecting observer gain matrix appropriately. Placing the eigenvalue of M in Left Half Plane (LHP), it is always possible to find a positive-definite matrix P such that

$$M^{\mathrm{T}}P + PM = -Q \tag{32}$$

for any given positive-definite matrix Q. Let λ_m denote the smallest eigenvalue of Q. Selecting a Lyapunov function

$$V_1(\tilde{z}) = \tilde{z}^{\mathrm{T}}P\tilde{z} \tag{33}$$

and computing the time derivative of Lyapunov function along (25) as

$$\dot{V}_1 = \tilde{z}^T(M^TP + PM)\tilde{z} + 2\tilde{z}^TPN\dot{e} \tag{34}$$

$$\dot{V}_1 \leqslant -\tilde{z}^TQ\tilde{z} + 2\|PN\|\|\tilde{z}\|\mu \tag{35}$$

$$\leqslant -\lambda_m\|\tilde{z}\|^2 + 2\|PN\|\|\tilde{z}\|\mu \tag{36}$$

$$\leqslant -\|\tilde{z}\|(\lambda_m\|\tilde{z}\| - 2\|PN\|\mu) \tag{37}$$

It can be seen that the asymptotic stability cannot be guaranteed but the $\|\tilde{z}\|$ cannot exceed a bound and therefore will remain ultimately bounded. Therefore, after a sufficiently long time, the norm of $\tilde{z}$ is bounded by

$$\|\tilde{z}\| \leqslant \lambda_1 \tag{38}$$

where

$$\lambda_1 = \frac{2\|PN\|\mu}{\lambda_m} \tag{39}$$

Next the bounds of $\hat{\sigma}$ is computed by taking the Lyapunov function as

$$V_2(\hat{\sigma}) = \frac{1}{2}\hat{\sigma}^2 \tag{40}$$

computing the time derivative of V_2 along (31) and (38)

$$\dot{V}_2 = -k\hat{\sigma}^2 + SLC\tilde{x}\sigma \tag{41}$$

$$\leqslant -|\hat{\sigma}| \cdot [k|\hat{\sigma}| - \|SLC\|\lambda_1] \tag{42}$$

therefore $\hat{\sigma}$ is bounded by

$$|\hat{\sigma}| \leqslant \lambda_2 \tag{43}$$

where

$$\lambda_2 = \frac{\|SLC\|\lambda_1}{k} \tag{44}$$

One can prove the boundedness of $\tilde{\sigma} = \sigma - \hat{\sigma}$ along similar lines. One can lower the bounds λ_1, λ_2 arbitrarily by appropriately selecting the observer gains and the control parameters.

Simulation and discussion

The effectiveness of the proposed scheme is assessed through simulation of the quarter-car suspension model given in Figure 1. The performance of the passive suspension system, the linear quadratic Gaussian (LQG) observer, the controller design based on IDC detailed in Section 3 and the design based on IDO given in Section 4.2 are compared for the same road profile. These are referred to as case I, II, III and IV in the sequel. Further the effect of changing the value of the sprung mass for the IDO-based controller is simulated, which is referred to as case V. The investigation with two more road profiles is referred to as case VI. All simulations were carried out in MATLAB/Simulink environment. The total space between the sprung and unsprung mass is known as the rattle space and is denoted by L. In the results, the plots of relative suspension deflection are the plots of the ratio of suspension deflection $(x_1 - x_3)$ to the rattle space L. The relative suspension deflection is denoted by ξ. The nominal values of the parameters of the suspension system considered for simulation are shown in Table 1.

Table 1. Nominal parameters considered for simulations.

Parameter	Value	Units
m_s	290	kg
m_{us}	59	kg
k_s	14500	N/m
b_s	1385.4	N/m s
b_{us}	170	N/m s
k_{us}	190,000	N/m
L	0.12	m

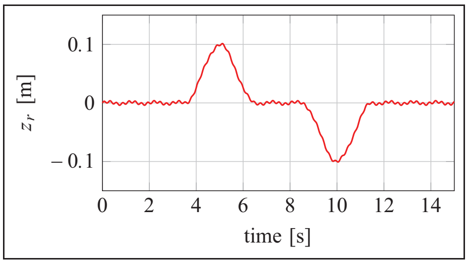

Figure 4. Road profile.

The road profile[38] used for simulation is shown in Figure 4. It is generated by the following:

$$z_r(t) = \begin{cases} -0.0592t_1^3 + 0.1332t_1^2 + dt; & 3.5 \leqslant t < 5 \\ 0.0592t_2^3 + 0.1332t_2^2 + dt; & 5 \leqslant t < 6.5 \\ 0.0592t_3^3 - 0.1332t_3^2 + dt; & 8.5 \leqslant t < 10 \\ -0.0592t_4^3 - 0.1332t_4^2 + dt; & 10 \leqslant t < 11.5 \\ d(t), & \text{otherwise} \end{cases} \tag{45}$$

where $d(t) = 0.002\sin(2\pi t) + 0.002\sin(7.5\pi t)$ is the sinusoidal disturbance and the time intervals are define as $t_1 = t - 3.5$, $t_2 = t - 6.5$, $t_3 = t - 8.5$ and $t_4 = t - 11.5$.

Case I: Passive suspension system

The simulation results obtained with the passive suspension system are shown in Figure 5 for the road profile described in (45). The plots of the acceleration of the sprung mass, the road disturbance and the sprung mass displacement, the sprung mass deflection and the relative suspension deflection are shown in Figure 5a, (b), (c) and (d), respectively. It can be seen from the plot of sprung mass displacement and the road disturbance that the sprung mass closely follows the road disturbance and consequently the sprung mass acceleration is moderately large.

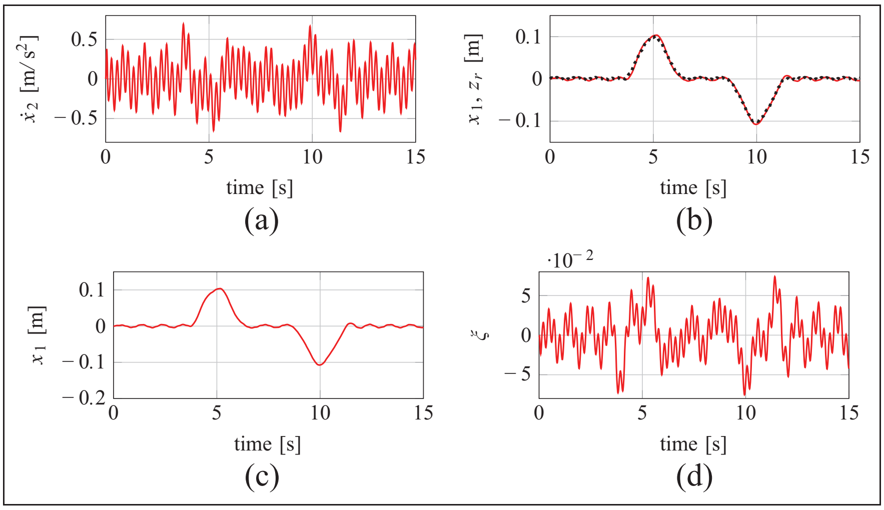

Figure 5. Simulation results with the passive suspension system (case I): (a) $\dot{x}_2$, (b) x_1 (solid line) and z_r (dashed), (c) x_1, (d) ξ.

Case II: Active suspension with LQG observer

In this case, an LQG observer[30]-based controller is designed and simulated. Since this methodology requires the full state of the system, the full state observer is designed using two measurements. The system states are selected as $q = [q_1\ q_2\ q_3\ q_4]^T$ where $q_1 = x_s - x_{us}$, $q_2 = \dot{x}_s$, $q_3 = x_{us} - z_r$, $q_4 = \dot{x}_{us}$. The dynamics of the system is mathematically represented as

$$\left.\begin{aligned} \dot{q} &= A_n q + B_n u \\ y &= C_n q \end{aligned}\right\} \tag{46}$$

The nominal parameters of the system are taken as

$$A_n = \begin{bmatrix} 0 & 1 & 0 & -1 \\ -50 & -4.777 & 0 & 4.777 \\ 0 & 0 & 0 & 1 \\ 245.76 & 23.48 & -3220.33 & -26.36 \end{bmatrix};$$

$$B_n = \begin{bmatrix} 0 & 0 \\ 0 & 0.0034 \\ -1 & 0 \\ 2.88 & -0.0169 \end{bmatrix};$$

$$C_n = \begin{bmatrix} 1 & 0 & 0 & 0 \\ -50 & -4.777 & 0 & 4.777 \end{bmatrix}$$

The dynamics of the observer is defined as

$$\dot{\hat{x}}_{\text{obs}} = A_n \hat{x}_{\text{obs}} + B_n u + L(y - \hat{y}) \tag{47}$$

$$\hat{y} = C_n \hat{x}_{\text{obs}} \tag{48}$$

where $\hat{x}_{\text{obs}}$ is the estimate of state vector and L is a Kalman gain which is computed from the matrices A_n, C_n.

The control input u is given by

$$u = -K\hat{x}_{obs} \tag{49}$$

where K is called a feedback gain matrix. The controller and observer gains are set to

$$K = \begin{bmatrix} 24.6 \\ 228.1 \\ -4216.7 \\ -120.5 \end{bmatrix}; L = \begin{bmatrix} 0.00094 & -0.233 \\ -0.00714 & -1.809 \\ -1.9516\times10^{-5} & 0.0105 \\ 0.026 & 6.361 \end{bmatrix}$$

The performance of the system such as the plots of the sprung mass acceleration, the comparative plots of the sprung mass displacement and the road profile, the displacement of sprung mass alone, the control input and the relative suspension deflection are shown in Figure 6(a)–(e). The comparative plots of the states and their estimation are shown in Figure 6f–(i). It can be seen that the estimations of the sprung mass and unsprung mass deflections are good but the estimations of the sprung mass and unsprung mass velocities are not good. The acceleration of the sprung mass is only slightly less as compared with the passive suspension system.

Case III: Active suspension based on SMC with and without IDC

In this case, active suspension based on SMC with IDC and without IDC is considered.

(a) Active suspension with IDC-based SMC

In this case, the results are obtained by assuming that the displacement and the velocity of the sprung mass are available for the controller design. The design of the sliding surface and the controller are as per (4), (8), (9) and (12). The parameters of this scheme are selected as $k = 10$, $\tau = 0.01$ and $c = 1$.

The results using this approach are shown in Figure 7. The plot of sprung mass acceleration, the comparative plot of sprung mass displacement and the road profile, the displacement of the sprung mass, the control input, the sliding variable and the relative suspension deflection are shown in Figure 4a–(f). The plot of the lumped uncertainty and its estimation are shown

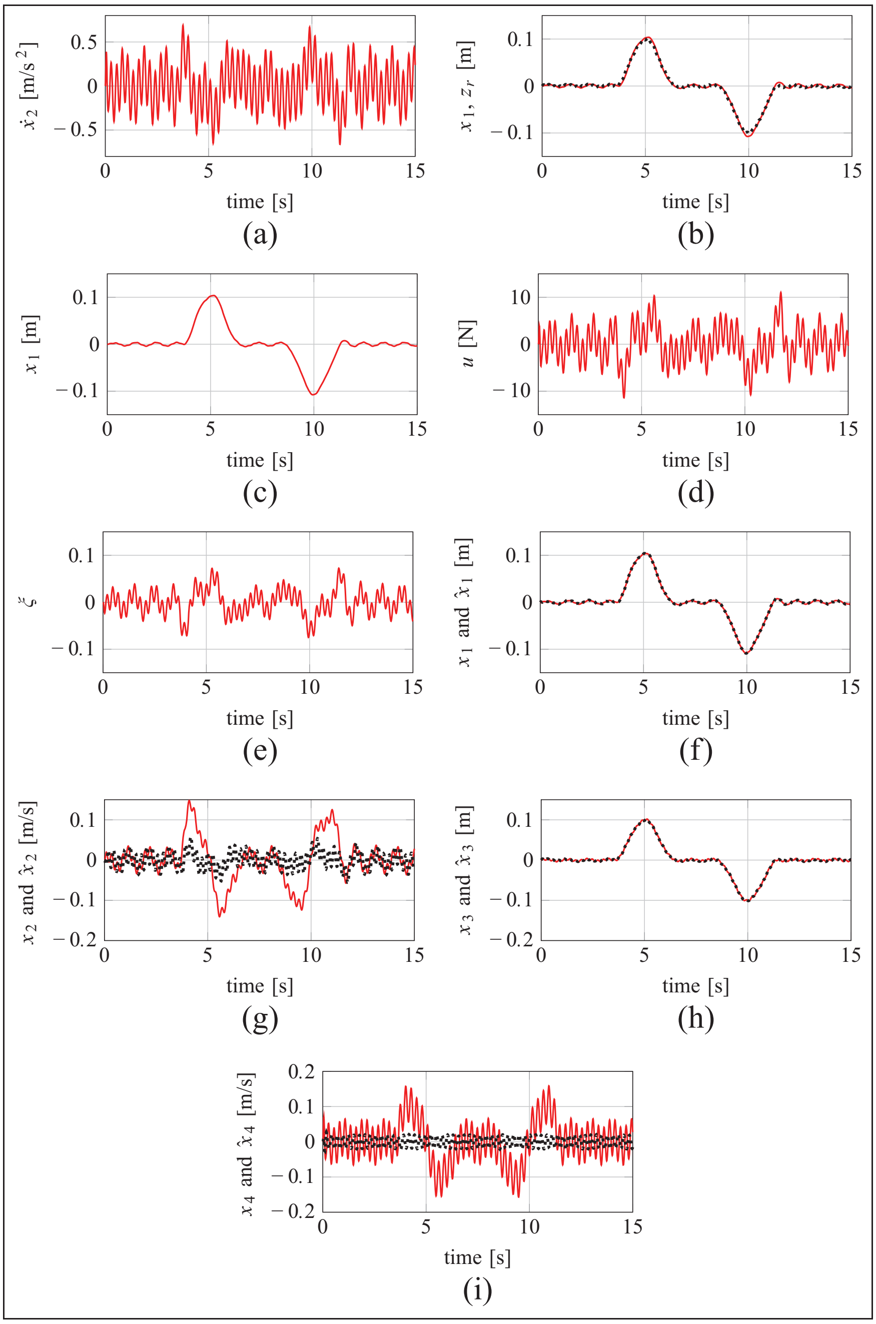

Figure 6. Simulation results with the LQG observer-based controller (case II): (a) $\dot{x}_2$, (b) x_1 (solid line) and z_r (dashed line), (c) x_1, (d) u, (e) ξ, (f) x_1 (solid line) and $\hat{x}_1$ (dashed line), (g) x_2 (solid line) and $\hat{x}_2$ (dashed line), (h) x_3 (solid line) and $\hat{x}_3$ (dashed line), (i) x_4 (solid line) and $\hat{x}_4$ (dashed line).

in Figure 7g. It can be observed that the estimation of the lumped uncertainty $\hat{e}$ is very close to the lumped uncertainty e. The acceleration obtained using this method is markedly low compared with the previous two cases. The relative suspension deflection is within the limit as can be seen from Figure 7f.

(b) Active suspension-based SMC without IDC: conventional SMC

In this case, the control is based on pure SMC, i.e. conventional SMC. For this case the control component u_n given in 30 is changed to

$$u_n = -(SB)^{-1} k_{dis}\, \mathrm{sat}(\sigma) \tag{50}$$

where k_{dis} is a positive constant and sat (σ) is defined as

$$\mathrm{sat}(\sigma) = \begin{cases} \mathrm{sgn}\ \sigma & |\sigma| > \epsilon \\ \dfrac{\sigma}{\epsilon} & |\sigma| \leqslant \epsilon \end{cases} \tag{51}$$

For this control to be effective, k_{dis} must be chosen so that it is greater than the maximum value of $|e|$. Since the uncertainty e is unknown, it is difficult to select k_{dis}. The simulations with three values of k_{dis} namely 1000, 1600 and 3000 were carried out. The plots of acceleration of sprung mass and the plots of the control signal

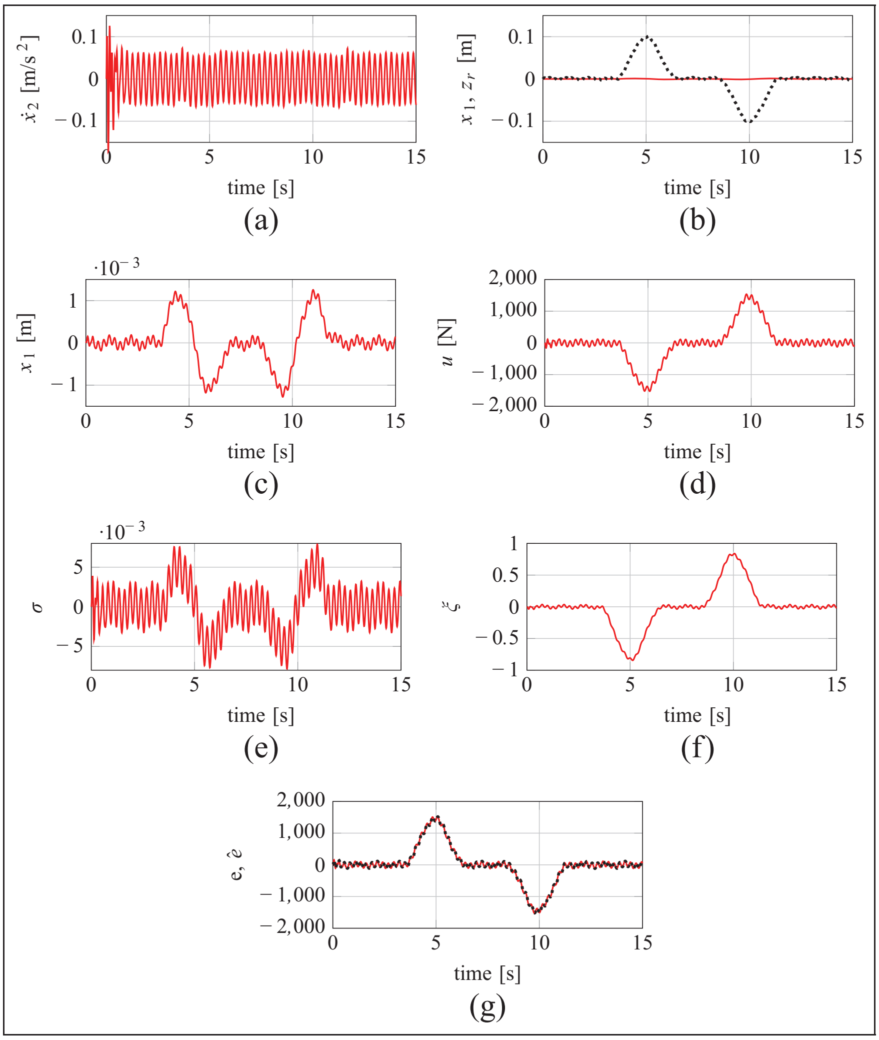

Figure 7. Simulation results for IDC-based SMC (case IIIa): (a) $\dot{x}_2$, (b) x_1 (solid line) and z_r (dashed line), (c) x_1, (d) u, (e) σ, (f) ξ, (g) e (solid line) and $\hat{e}$ (dashed line).

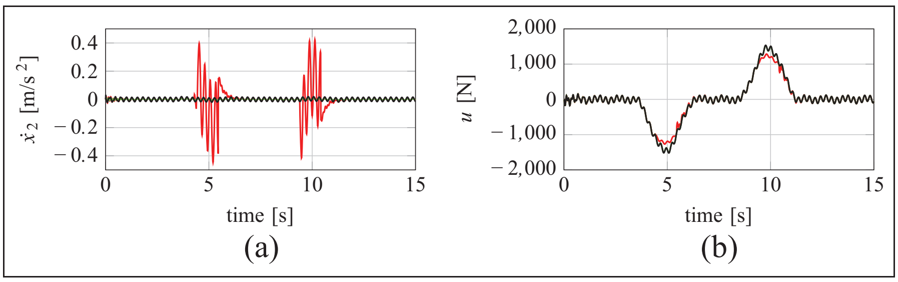

Figure 8. Simulation results with conventional SMC (case IIIb): $k_{dis} = 1000$ (red color), $k_{dis} = 1600$ (black color) and $k_{dis} = 3000$ (green color): (a) $\dot{x}_2$, (b) u.

are shown Figure 8a and (b), respectively. It may be noted that it is difficult to select k_{dis} for different unknown road profiles.

Case IV: Active suspension with IDO-based SMC

In this case, the IDO is used to estimate the states and the disturbances using the measurement of the sprung mass position alone. The IDO is designed using (17), (21), placing the observer poles at $[-100 \pm 200j\ -100]$. The controller is designed using (28), (29) and (30) keeping the parameters the same as in case III.

The results with IDO-based SMC are given in Figure 9. The magnitude of the sprung mass deflection in Figure 9c and the acceleration in Figure 9a are almost

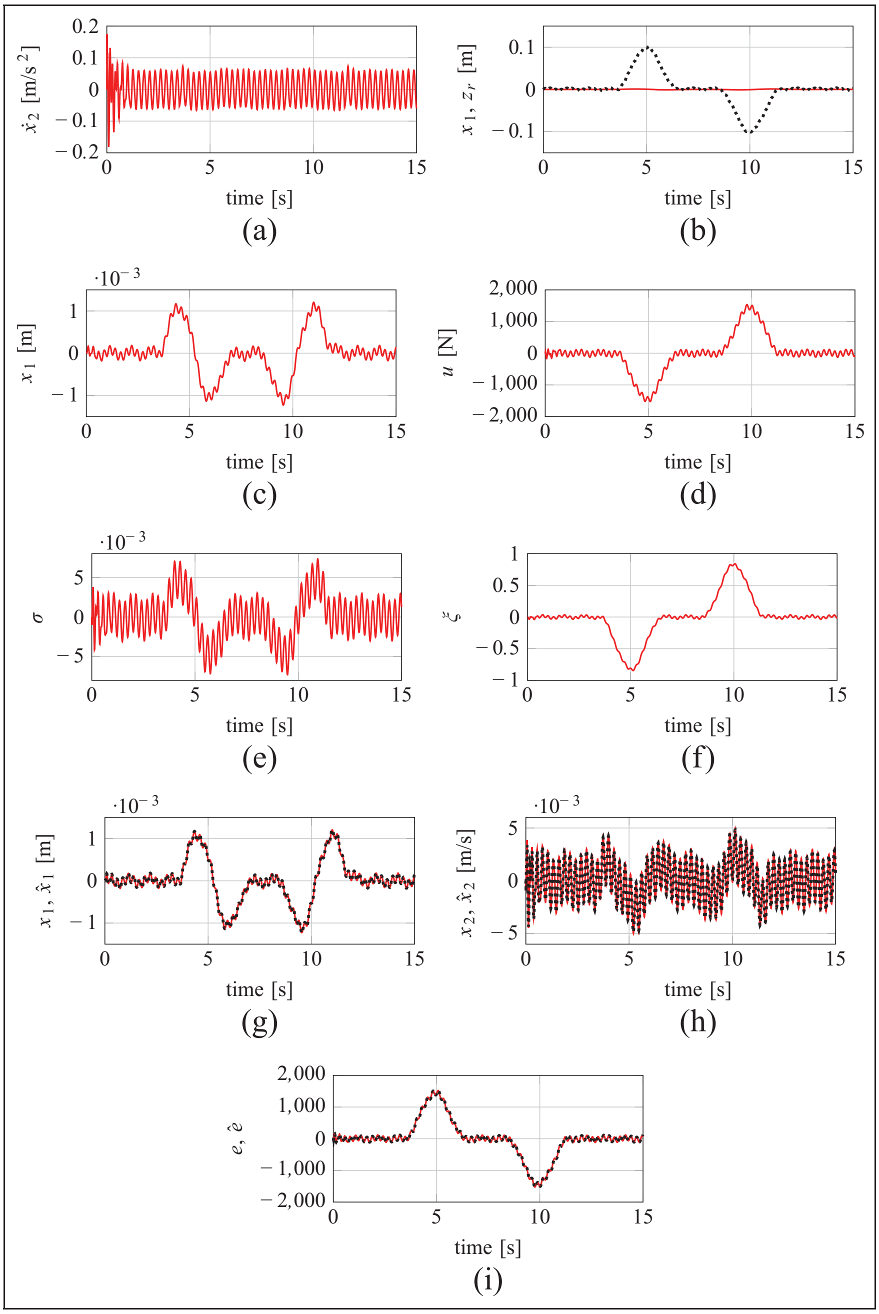

Figure 9. Simulation results with IDO-based SMC (case IV): (a) $\dot{x}_2$, (b) x_1 (solid line) and z_r (dashed line), (c) x_1, (d) u, (e) σ, (f) ξ, (g) x_1 (solid line) and $\hat{x}_1$ (dashed line), (h) x_2 (solid line) and $\hat{x}_2$ (dashed line), (i) e (solid line) and ê (dashed line).

same as those obtained in case III. The estimation of the states and the lumped uncertainty are shown in Figure 9g, (h) and (i), respectively. It may be noted that the IDO is successful in estimating the sprung mass velocity x_2. So the objective of estimating the states and the uncertainty is fulfilled.

The maximum and root-mean-square (RMS) values of the displacement and the acceleration of the sprung mass for all four cases are shown in Table 2. It can be seen that the performance of active suspension system in terms of displacement and acceleration of the sprung mass for case III (IDC-based controller) and case IV (IDO-based controller) are significantly better then case I (passive) and case II (LQG observer). The performance of the IDC-based controller and the IDO-based controller are very close to each other but the IDO-based controller requires only one measurement. Thus the IDO-based controller saves one sensor without compromising the system performance.

For a better visual comparison of results of cases I–IV, the sprung mass acceleration, sprung mass displacement, control and the relative suspension deflection for the four cases superimposed on each other are shown in Figure 10a–(d), respectively.

Table 2. Maximum and RMS values comparison of simulation results.

Case	Types of suspension	Displacement (m)		Acceleration (m/s^2)	
		Max	RMS	Max	RMS
I	Passive	0.1037	0.0399	0.6908	0.2628
II	LQG observer	0.1038	0.04	0.6893	0.2661
III a	SMC with IDC	0.0013	5.2438×10^{-4}	0.1262	0.0444
IV	SMC with IDO	0.0012	5.029×10^{-4}	0.1989	0.0447

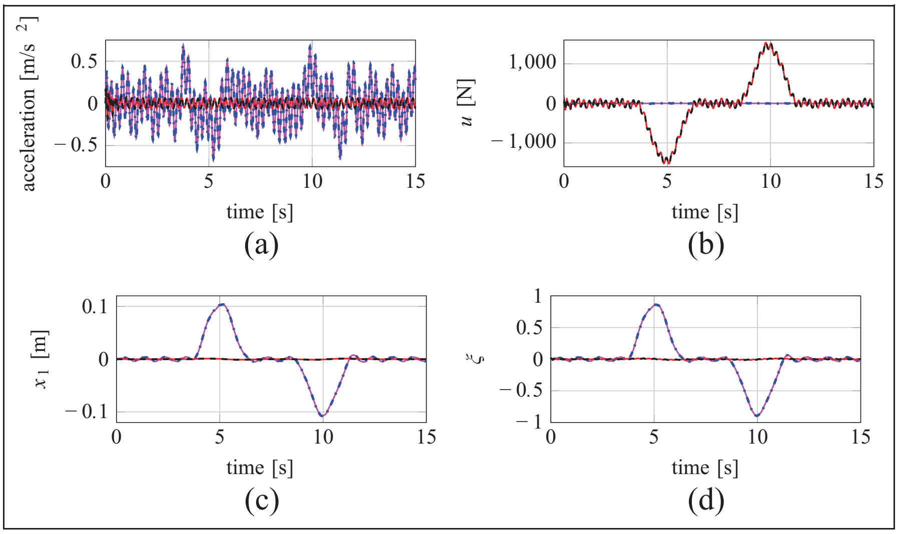

Figure 10. Comparative simulation results of case I (pink solid line), case II (blue dash dotted line), case III a (black dashed line) and case IV (red solid line): (a) $\dot{x}_2$, (b) x_1, (c) u, (d) ξ.

Table 3. Performance for sprung mass = 350 kg: maximum and RMS values comparison of simulation results (case V).

Types of suspension	Displacement (m)		Acceleration (m/s^2)	
	Max	RMS	Max	RMS
Passive	0.1034	0.0402	0.6081	0.2368
SMC with IDC	0.001	4.3518×10^{-4}	0.1049	0.0369
SMC with IDO	0.001	4.1830×10^{-4}	0.1906	0.0375

Table 4. Performance for sprung mass = 230 kg: maximum and RMS values comparison of simulation results (case V).

Types of suspension	Displacement (m)		Acceleration (m/s^2)	
	Max	RMS	Max	RMS
Passive	0.1033	0.0396	0.7955	0.3077
SMC with IDC	0.0016	6.5955×10^{-4}	0.1581	0.0556
SMC with IDO	0.0015	6.3034×10^{-4}	0.2114	0.0555

Case V: Active suspension with varying load

In this case, the sprung mass is assumed to be uncertain as the number of passengers may vary in a typical passenger car. For this case the results are obtained assuming $\pm$ 20% uncertainty in the sprung mass.

The performance of the passive suspension system, IDC-based SMC and IDO based SMC are shown in Tables 3 and 4 for sprung mass having a value of 350 and 230 kg, respectively. It can be seen from the tables that the performance of the passive system is affected significantly due to the change in mass. However the

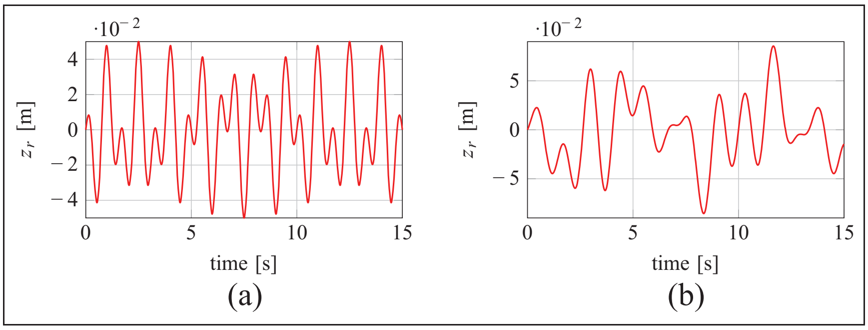

Figure 11. Road profiles (a) and (b).

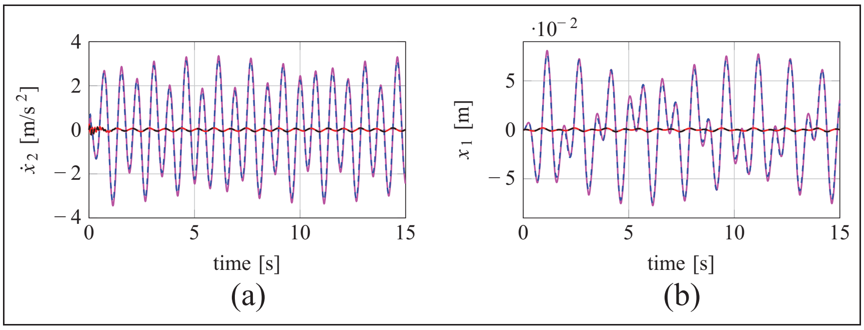

Figure 12. Comparative simulation results of case I (pink solid line), case II (blue dash-dotted line), case III a (black dashed line) and case IV (red solid line) for road profile (a): (a) $\dot{x}_2$; (b) x_1.

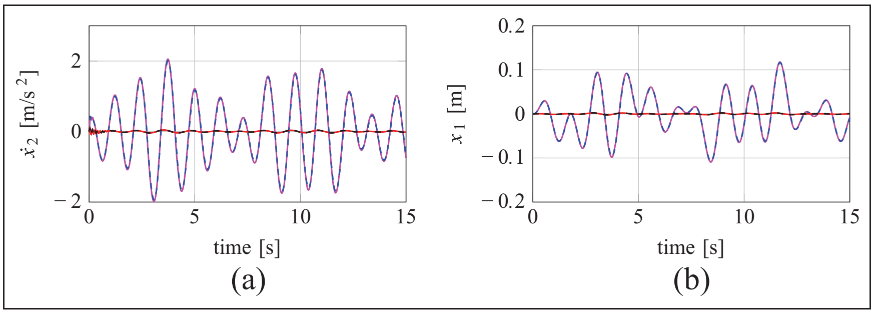

Figure 13. Comparative simulation results of case I (pink solid line), case II (blue dash dotted line), case IIIa (black dashed line) and case IV (red solid line) for road profile (b): (a) $\dot{x}_2$; (b) x_1.

IDC- and IDO-based schemes are almost unaffected by the change in the sprung mass.

Case VI: Active suspension with other road profiles

In order to assess the effectiveness of the proposed control for other road profiles, simulation was carried out for the following road profiles: road profile (a) $z_r = 0.05\cos(2\pi t)\sin(0.6\pi t)$ and road profile (b) $z_r = 0.05\sin(1.5\pi t)\sin(0.15\pi t) + 0.05\cos(0.6\pi t)\sin(0.3\pi t)$. The plots of road profile (a) and (b) are shown in Figure 11a and (b), respectively. The comparison of the proposed scheme with passive, LQG observer, IDC-based SMC is plotted in Figure 12 for road profile (a) and in Figure 13 for road profile (b) and the results are tabulated in Tables 5 and 6. The results confirm the superiority of the proposed scheme over passive and LQG observer for these profiles as well.

Experimental results

For validation of the proposed scheme and the other methods mentioned in the previous section, these are implemented on an actual hardware setup in laboratory for the same kind of road profile. The laboratory setup[39] shown in Figure 14, is a bench-scale model to emulate a quarter-car model, which consists of a sprung mass (top blue plate), an unsprung mass (middle red plate), an actuator and a road simulator (bottom silver plate). The actuator, which is a DC motor, is

Table 5. Performance for road profile (a): maximum and RMS values comparison of simulation results (case VI).

Types of suspension	Displacement (m)		Acceleration (m/s^2)	
	Max	RMS	Max	RMS
Passive	0.0808	0.0389	3.4434	1.9129
LQG observer	0.0770	0.0375	3.2618	1.8092
SMC with IDC	0.0020	9.9007×10^{-4}	0.2116	0.0535
SMC with IDO	0.0019	9.5392×10^{-4}	0.3551	0.0532

Table 6. Performance for road profile (b): maximum and RMS values comparison of simulation results (case VI).

Types of suspension	Displacement (m)		Acceleration (m/s^2)	
	Max	RMS	Max	RMS
Passive	0.1177	0.0479	2.0543	0.9456
LQG observer	0.1163	0.0472	2.0085	0.9185
SMC with IDC	0.0023	0.0010	0.0962	0.0219
SMC with IDO	0.0022	9.8880×10^{-4}	0.0956	0.0219

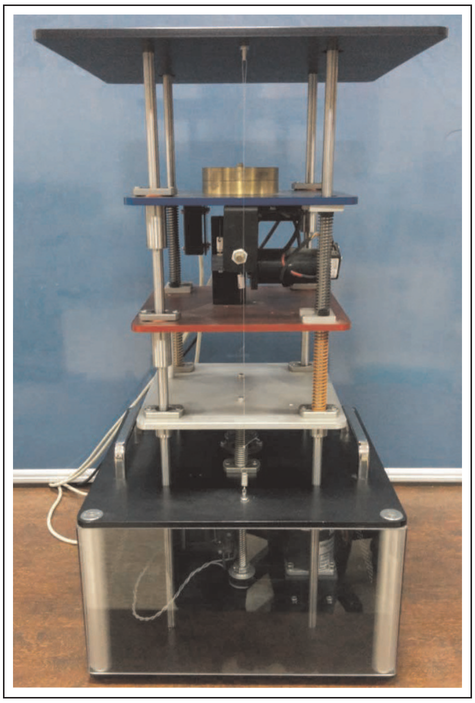

Figure 14. Laboratory setup.

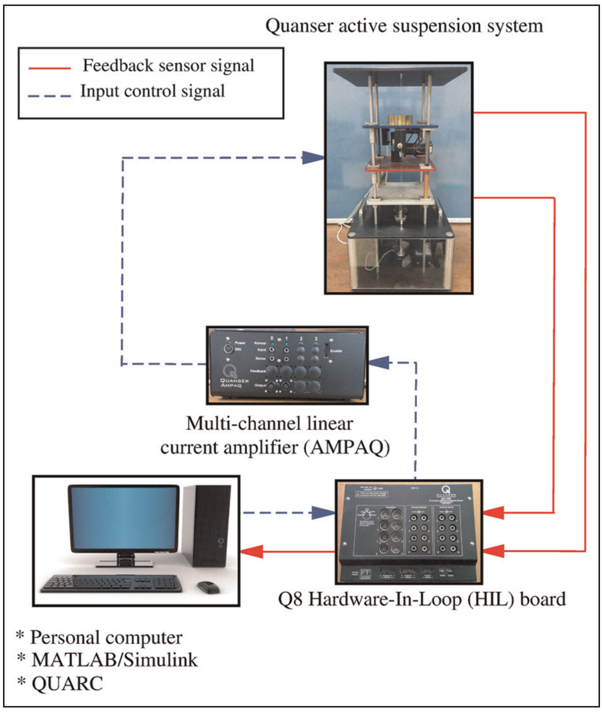

Figure 15. Implementation scheme of hardware setup.

placed between the sprung mass and the unsprung mass in parallel with a spring and a damper. An accelerometer and an optical encoder are connected to the sprung mass to measure the acceleration and the position of the sprung mass. The bottom plate is servo controlled by a DC motor which simulates different types of road disturbances. The sprung mass position is sensed using a 10-bit optical encoder and there is no sensor for velocity measurement. Apart from these components, the hardware set-up consists of a power amplifier and a data acquisition card to provide interface between a Personal computer and the hardware. The schematic diagram of the implementation of the whole system is shown in Figure 15. The controller can be designed in the MATLAB/Simulink environment first with a simulated plant and then with the active suspension system shown in Figure 14. The nominal parameters of the experimental set-up are given in Table 7.

The experimental results were obtained for case I (passive system), case II (LQG observer-based control), case III (IDC-based controller) and case IV (IDO-based controller).

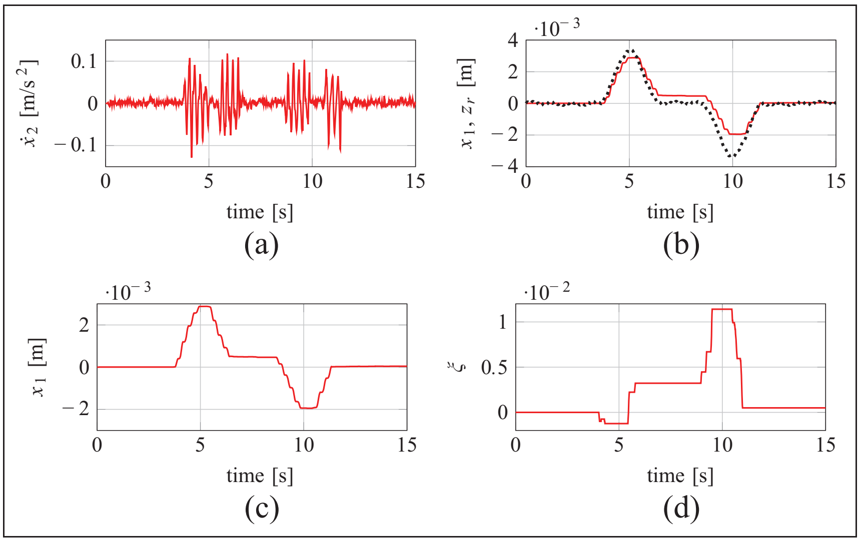

Figure 16. Experimental results for passive suspension system: (a) $\dot{x}_2$, (b) x_1 (solid line) and z_r (dashed), (c) x_1, (d) ξ.

Table 7. Parameters of experimental setup.

Parameter	Value	Units
m_s	2.45	kg
m_u	1	kg
k_s	900	N/m
b_s	7.5	N/m s
b_{us}	5	N/m s
k_{us}	1250	N/m
L	0.038	m

Case I: Passive suspension system

The results for this case are shown in Figure 16. It can be observed that with passive system, the sprung mass follows the road excitation like the corresponding results in the simulation.

Case II: Active suspension with LQG observer-based control

The results for this case are shown in Figure 17. It can be seen that as far as the sprung mass acceleration is concerned, the results are better then the passive suspension system by nearly a factor of two. The state estimation shows noticeable errors.

Case III: Active suspension with IDC-based SMC

In this case, the sprung mass displacement is measured by an optical encoder while the velocity of the sprung mass is obtained from the sprung mass displacement by passing it through a high-pass filter having a transfer function

$$H_f(s) = \frac{s\omega_n^2}{s^2 + 2\zeta\omega_n s + \omega_n^2} \tag{52}$$

with $w_n = 100$ and $\zeta = 1$. The results are shown in Figure 18. One can observe the fluctuation in the acceleration of the sprung mass during 4–6 seconds and 9–11 seconds. The deflection of the sprung mass is less as compared with the previous two cases. The plot of the lumped uncertainty estimation $\hat{e}$ is shown in Figure 18g. Obtaining the velocity by passing the optical encoder signal through the high-pass filter (52), has resulted in a deterioration in the ride comfort.

Case IV: Active suspension with IDO-based SMC

Lastly the results with IDO based SMC are shown in Figure 19. The plot of acceleration of the sprung mass is shown in Figure 19a where the magnitude is very small as compared with all three previous cases. The signals of the system such as the sprung mass displacement and the road disturbance profile together, the sprung mass displacement, the control input, the sliding surface and the relative suspension deflection are shown in Figure 19b–(f), respectively. The estimate of the states and the lumped uncertainties are shown in Figure 19g, (h) and (i), respectively. It can be observed from Figure 19h that there is a marked difference between the velocity signal provided by the high pass filter and the one estimated by IDO. The improvement in the ride comfort obtained in this case in comparison with the case III (IDC-based controller) can be attributed to the better estimation of x_2. Worthy of note are the plots of the sliding surface σ, Figure 18e and (e) for the IDC and the IDO cases. The sliding variable sigma, which is a measure of the performances of the systems, is smaller for the IDO case indicating its better performance.

The performance of the system with all cases are summarized in Table 8. It can be seen from Table 8 that the system with IDO-based SMC gives a remarkable improvement in the ride comfort compared to all other cases. Among all of the results of passive, LQG

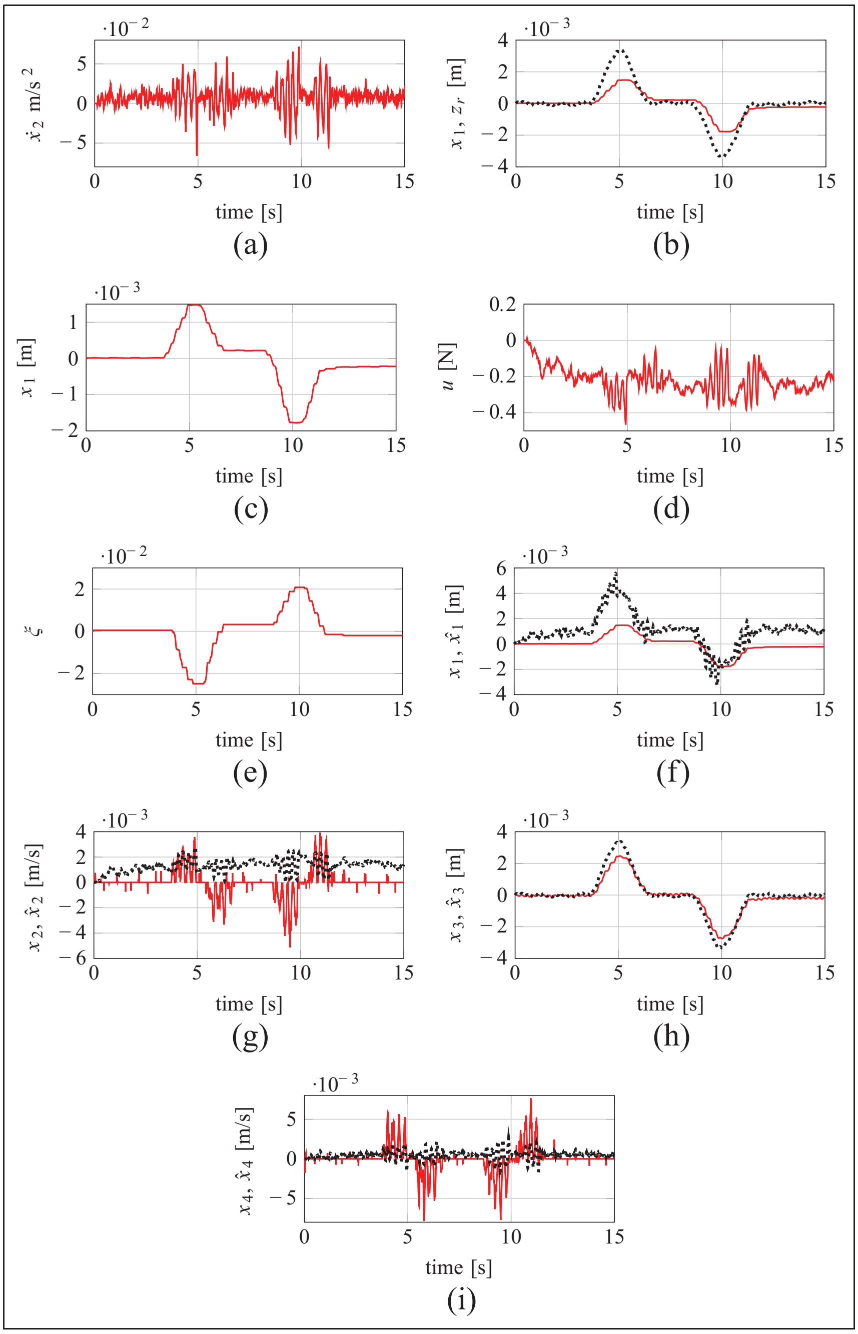

Figure 17. Experimental results for LQG observer-based control: (a) $\dot{x}_2$, (b) x_1 (solid line) and z_r (dashed line), (c) x_1, (d) u, (e) ξ, (f) x_1 (solid line) and $\hat{x}_1$ (dashed line), (g) x_2 (solid line) and $\hat{x}_2$ (dashed line), (h) x_3 (solid line) and $\hat{x}_3$ (dashed), (i) x_4 (solid line) and $\hat{x}_4$ (dashed line).

Table 8. Maximum and RMS values comparison of hardware results.

Case	Types of suspension	Displacement (m)		Acceleration (m/s^2)	
		Max	RMS	Max	RMS
I	Passive	0.0029	0.001	0.1212	0.0276
II	LQG observer	0.0015	6.9206×10^{-4}	0.0731	0.0166
III	SMC with IDC	2.6787×10^{-4}	8.4250×10^{-5}	0.1375	0.0156
IV	SMC with IDO	1.4611×10^{-4}	7.5986×10^{-5}	0.0236	0.0065

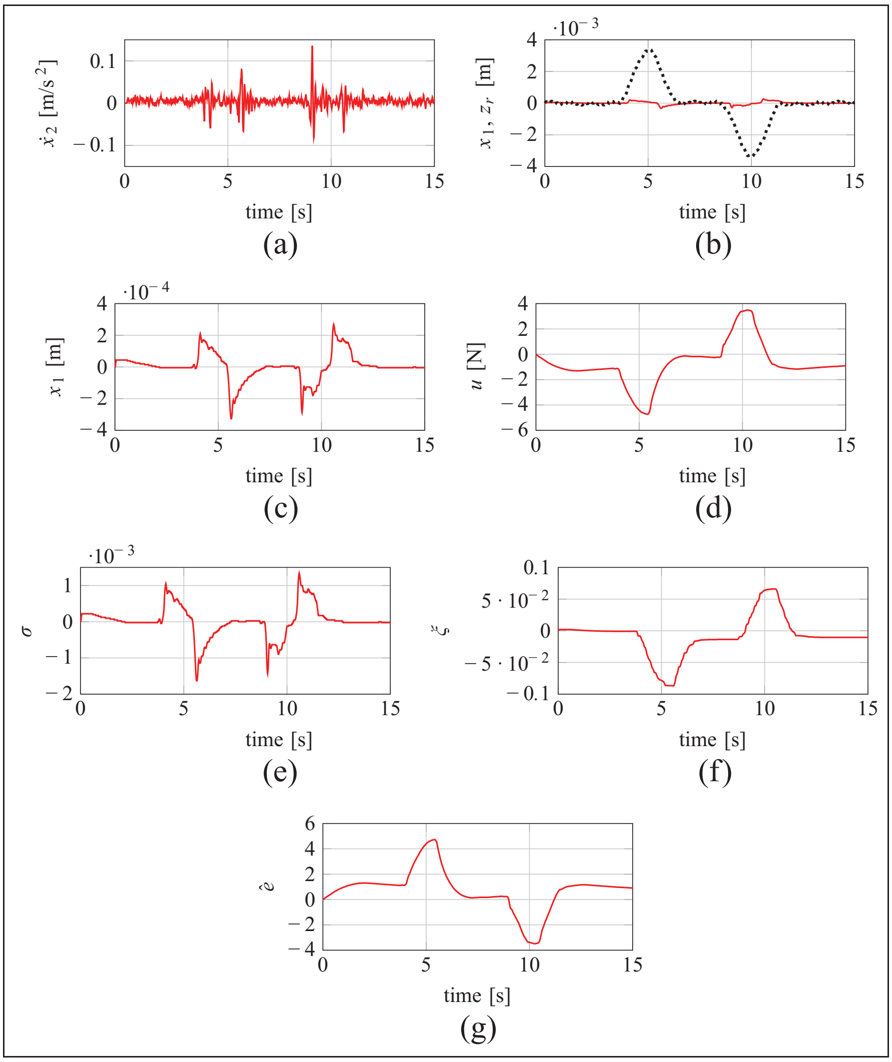

Figure 18. Experimental results for IDC-based SMC: (a) $\dot{x}_2$, (b) x_1 (solid line) and z_r (dashed), (c) x_1, (d) u, (e) σ, (f) ξ, (g) $\hat{e}$.

observer based control, IDC-based SMC and IDO-based SMC, the RMS values of the displacement and the acceleration of the sprung mass obtained with IDO-based SMC are the least. In the case of IDO-based SMC, the sprung mass acceleration is reduced by a factor of five as compared with the passive case. It may be noted that the sprung mass position is obtained using an optical encoder. In the IDC approach, the sprung mass velocity is obtained by differentiating the encoder signal by means of a high-pass filter while in the IDO-based approach, it is obtained through the use of a robust observer. This is why the hardware results with IDC are poorer as compared with those with IDO.

Case V: Active suspension with IDO-based SMC with sprung mass variation

The controller with IDO was tested for three values of sprung mass namely $m_s = 0.2$, 1.2 and 2.45 kg. The results of sprung mass acceleration and the control are shown in Figure 20a and (b), respectively. It can be seen that the proposed scheme is robust to significant uncertainties in the sprung mass.

Conclusion

In this paper, an IDO-based active suspension system which estimates the effect of uncertainties, unknown road profiles and the states of the sprung mass is proposed. The proposed scheme is successful in giving ride comfort using only one sensor. The scheme is validated by simulation and experimentation on a laboratory hardware setup. The results obtained with the proposed scheme are compared with a passive suspension system, an LQG observer based suspension system and an IDC-based suspension system. The scheme gives better ride comfort than the passive and the LQG observer based control. The comparison of the simulation results show that the proposed scheme gives a performance that is as good as that obtained with the IDC-based

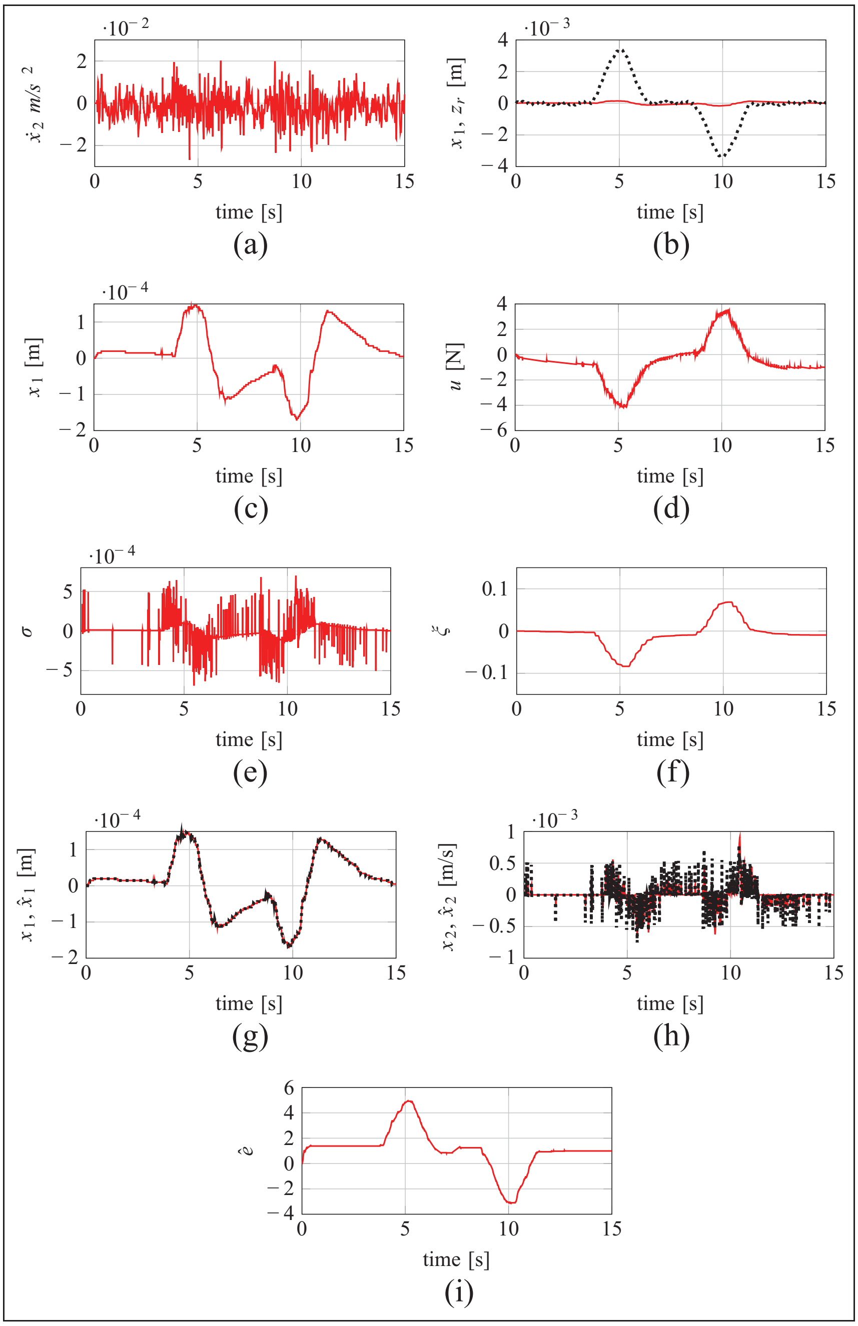

Figure 19. Experimental results for IDO-based SMC: (a) $\dot{x}_2$, (b) x_1 (solid line) and z_r (dashed), (c) x_1, (d) u, (e) σ, (f) ξ, (g) x_1 (solid line) and $\hat{x}_1$ (dashed), (h) x_2 (solid line) and $\hat{x}_2$ (dashed), (i) $\hat{e}$.

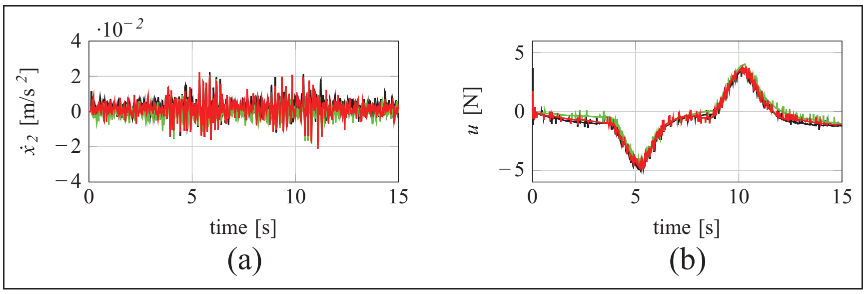

Figure 20. Experimental results for IDO-based SMC with sprung mass variations, $m_s = 0.2$ kg (red color), 1.2 kg (green color), 2.45 kg (black color): (a) $\dot{x}_2$, (b) u.

scheme while needing one sensor less. However the comparison of the hardware results obtained with proposed scheme are better than the IDC-based scheme.

References

[1] Hrovat D. Applications of optimal control to advanced automotive suspension design. *J Dynam Syst Meas Control* 1993; 115(2B): 328–342.
[2] Chen S, He R, Liu H et al. Probe into necessity of active suspension based on LQG control. *Phys Procedia* 2012; 25: 932–938.
[3] Fialho I and Balas GJ. Road adaptive active suspension design using linear parameter-varying gain-scheduling. *IEEE Trans Control Syst Technol* 2002; 10(1): 43–54.
[4] Alleyne A and Hedrick JK. Nonlinear adaptive control of active suspensions. *IEEE Trans Control Syst Technol* 1995; 3(1): 94–101.
[5] Rajamani R and Hedrick JK. Adaptive observers for active automotive suspensions: theory and experiment. *IEEE Trans Control Syst Technol* 1995; 3(1): 86–93.
[6] Truscott A. Composite active suspension for automotive vehicles. *Comput Control Eng J* 1994; 5(3): 149–154.
[7] Sunwoo M, Cheok KC and Huang N. Model reference adaptive control for vehicle active suspension systems. *IEEE Trans Indust Electron* 1991; 38(3): 217–222.
[8] Mohan B and Phadke SB. Variable structure active suspension system. In *International conference on industrial electronics, control, and instrumentation*, volume 3. IEEE, pp. 1945–1948.
[9] Mohan B, Modak J and Phadke SB. Vibation control of vehicles using model reference adaptive variablestructure control. *Adv Vibr Eng* 2003; 2(4): 343–361.
[10] Zhao W, Wang C, Zhao T et al. Research on the multidisciplinary design method for an integrated automotive steering and suspension system. *Proc IMechE D J Automob Eng* 2014. DOI: 10.1177/0954407014559565.
[11] Her H, Suh J and Yi K. Integrated control of the differential braking, the suspension damping force and the active roll moment for improvement in the agility and the stability. *Proc IMechE D J Automob Eng* 2014. DOI: 10.1177/0954407014550502.
[12] Rajeswari K and Lakshmi P. Simulation of suspension system with intelligent active force control. In *International conference on advances in recent technologies in communication and computing*, pp. 271–277.
[13] Al-Holou N, Lahdhiri T, Joo DS et al. Sliding mode neural network inference fuzzy logic control for active suspension systems. *IEEE Trans Fuzzy Syst* 2002; 10(2): 234–246.
[14] Esat II, Saud M and Naci Engin S. A novel method to obtain a real-time control force strategy using genetic algorithms for dynamic systems subjected to external arbitrary excitations. *J Sound Vibr* 2011; 330(1): 27–48.
[15] Kim C and Ro P. A sliding mode controller for vehicle active suspension systems with non-linearities. *Proc IMechE D J Automob Eng* 1998; 212(2): 79–92.
[16] Lin J, Lian RJ, Huang CN et al. Enhanced fuzzy sliding mode controller for active suspension systems. *Mechatronics* 2009; 19(7): 1178–1190.
[17] Lian RJ. Enhanced adaptive self-organizing fuzzy sliding-mode controller for active suspension systems. *IEEE Trans Indust Electron* 2013; 60(3): 958–968.
[18] Deshpande VS, Shendge PD and Phadke SB. Active suspension systems for vehicles based on a sliding-mode controller in combination with inertial delay control. *Proc IMechE D J Automob Eng* 2013; 227(5): 675–690.
[19] Deshpande VS, Mohan B, Shendge PD et al. Disturbance observer based sliding mode control of active suspension systems. *J Sound Vibr* 2014; 333(11): 2281–2296.
[20] Williams R. Automotive active suspensions part 1: basic principles. *Proc IMechE D J Automob Eng* 1997; 211(6): 415–426.
[21] Preumont A, François A, Bossens F et al. Force feedback versus acceleration feedback in active vibration isolation. *J Sound Vibr* 2002; 257(4): 605–613.
[22] Alshehri A, Gardonio P, Elliott S et al. Experimental evaluation of a two degree of freedom capacitive MEMS sensor for velocity measurements. *Procedia Eng* 2011; 25: 619–622.
[23] Abdel-Hady M. Active suspension with preview control. *Vehicle System Dynamics* 1994(23); 1–13.
[24] Ryu S, Park Y and Suh M. Ride quality analysis of a tracked vehicle suspension with a preview control. *J Terramech* 2011; 48: 409–417.
[25] Rahman M and Rideout G. Using the lead vehicle as preview sensor in convoy vehicle active suspension control. In: *Vehicle System Dynamics* 2012(50); 1923–1948.
[26] Hedrick J, Rajamani R and Yi K. Observer design for electronic suspension applications. *Vehicle System Dynamics* 1994; 23(1): 413–440.
[27] Dixit RK and Buckner GD. Sliding mode observation and control for semiactive vehicle suspensions. *Vehicle System Dynamics* 2005; 43(2): 83–105.
[28] Chadli M, Rabhi A and El Hajjaji A. Observer-based $H\infty$ fuzzy control for vehicle active suspension. In *16th Mediterranean conference on control and automation*, pp. 1393–1398.
[29] Cheng CP, Chao CH and Li T. Design of observer-based fuzzy sliding-mode control for an active suspension system with full-car model. In *IEEE international conference on systems man and cybernetics*, pp. 1939–1944.
[30] Taghirad HD and Esmailzadeh E. Automobile passenger comfort assured through lqg/lqr active suspension. *J Vibr Control* 1998; 4(5): 603–618.
[31] Seo J, Shin D, Yi K et al. Control of the motorized active suspension damper for good ride quality. *Proc IMechE D J Automob Eng* 2014;: DOI: 10.1177/0954407014531246.
[32] Youcef-Toumi K and Ito O. A time delay controller for systems with unknown dynamics. *J Dynam Syst Meas Control* 1990; 112(1): 133–142.
[33] Zhong QC and Rees D. Control of uncertain LTI systems based on an uncertainty and disturbance estimator. *J Dynam Syst Meas Control* 2004; 126(4): 905–910.
[34] Talole SE and Phadke SB. Model following sliding mode control based on uncertainty and disturbance estimator. *J Dynam Syst Meas Control* 2008; 130(3): 034501.
[35] Phadke SB and Talole SE. Sliding mode and inertial delay control based missile guidance. *IEEE Trans Aerospace Electron Syst* 2012; 48(4): 3331–3346.
[36] Ginoya DL, Patel TR, Shendge PD et al. Design and hardware implementation of model following sliding mode control with inertial delay observer for uncertain systems. In *3rd international conference on electronics computer technology*, vol. 3, pp. 192–196.

[37] Corless M and Leitmann G. Continuous state feedback guaranteeing uniform ultimate boundedness for uncertain dynamic systems. *IEEE Trans Automatic Control* 1981; 26(5): 1139–1144.
[38] Chen PC and Huang AC. Adaptive sliding control of non-autonomous active suspension systems with time-varying loadings. *J Sound Vibr* 2005; 282(3): 1119–1135.
[39] Quanser Active Suspension system user manual. Quanser, 2010, pp. 3–5.

Appendix

Notation

m_s:	sprung mass
m_{us}:	unsprung mass
b_s:	sprung mass damper coefficient
b_{us}:	unsprung mass damper coefficient
k_s:	sprung mass spring stiffness
k_{us}:	unsprung mass spring stiffness
x_s:	displacement of the sprung mass
x_{us}:	displacement of the unsprung mass
z_r:	road profile relative to plane ground
u:	control force generated by the actuator
x_i:	states of the suspension system
y:	output of the suspension system
σ:	sliding surface
τ:	time constant of the inertial delay filter
μ:	positive constant
$\tilde{z}$:	observer error dynamics
c:	positive constant
e:	lumped uncertainty
$\hat{e}$:	estimate of the lumped uncertainty
$\tilde{e}$:	estimate error in lumped uncertainty
M:	constant matrix
P:	positive-definite matrix
Q:	positive-definite matrix
A, B, C:	system parameter matrices
$\hat{\sigma}$:	estimate of the sliding surface
$\tilde{\sigma}$:	error in estimation of the sliding surface
$\hat{x}$:	estimate of the states x
$\hat{y}$:	estimate of the output y
S:	constant row vector
q_i:	LQG observer states
K:	feedback gain matrix
L:	inertial delay observer gain matrix
L_k:	Kalman gain matrix
B^+:	pseudo–inverseofmatrix B
λ_1:	positive constant
λ_2:	positive constant
λ_m:	positive constant
A_n, B_n, C_n:	nominal system coefficient matrix, input and output matrix
$G_f(s)$:	inertial delay filter
$H_f(s)$:	second-order high-pass filter
$\hat{x}_{obs}$:	LQG observer states
L:	total space between sprung and unsprung mass
ξ:	relative suspension deflection